JVI Journals.ASM.org

Classical Swine Fever Virus p7 Protein Is a Viroporin Involved in Virulence in Swine

Douglas P. Gladue,[a] Lauren G. Holinka,[a] Eneko Largo,[d] Ignacio Fernandez Sainz,[a] Consuelo Carrillo,[f] Vivian O'Donnell,[a,b] Ryan Baker-Branstetter,[a] Zhiqiang Lu,[c] Xavier Ambroggio,[e] Guillermo R. Risatti,[b] Jose L. Nieva,[d] and Manuel V. Borca[a]

Plum Island Animal Disease Center, Agricultural Research Service, U.S. Department of Agriculture, Greenport, New York, USA[a]; Department of Pathobiology and Veterinary Science, University of Connecticut, Storrs, Connecticut, USA[b]; Plum Island Animal Disease Center, DHS, Greenport, New York, USA[c]; Biophysics Unit (CSIC-UPV/EHU) and Department of Biochemistry and Molecular Biology, University of the Basque Country (UPV/EHU), Bilbao, Spain[d]; Bioinformatics and Computational Biosciences Branch, National Institute of Allergy and Infectious Diseases, National Institutes of Health, Bethesda, Maryland, USA[e]; and Plum Island Animal Disease Center, APHIS, U.S. Department of Agriculture, Greenport, New York, USA[f]

The nonstructural protein p7 of classical swine fever virus (CSFV) is a small hydrophobic polypeptide with an apparent molecular mass of 6 to 7 kDa. The protein contains two hydrophobic stretches of amino acids interrupted by a short charged segment that are predicted to form transmembrane helices and a cytosolic loop, respectively. Using reverse genetics, partial in-frame deletions of p7 were deleterious for virus growth, demonstrating that CSFV p7 function is critical for virus production in cell cultures. A panel of recombinant mutant CSFVs was created using alanine scanning mutagenesis of the p7 gene harboring sequential three- to six-amino-acid residue substitutions spanning the entire protein. These recombinant viruses allowed the identification of the regions within p7 that are critical for virus production *in vitro*. *In vivo*, some of these viruses were partially or completely attenuated in swine relative to the highly virulent parental CSFV Brescia strain, indicating a significant role of p7 in CSFV virulence. Structure-function analyses in model membranes emulating the endoplasmic reticulum lipid composition confirmed that CSFV p7 is a pore-forming protein, and that pore-forming activity resides in the C-terminal transmembrane helix. Therefore, p7 is a viroporin which is clearly involved in the process of CSFV virulence in swine.

Classical swine fever (CSF) is a highly contagious often lethal disease of swine. The etiological agent, CSF virus (CSFV), is a small enveloped virus with a positive single-stranded RNA genome and, along with bovine viral diarrhea virus (BVDV) and border disease virus (BDV), is classified as a member of the genus *Pestivirus* within the family *Flaviviridae* (3). The 12.3-kb CSFV genome contains a single open reading frame that encodes a 3,898-amino-acid polyprotein that yields up to 12 final cleavage products (NH_2-Npro-C-E^{rns}-E1-E2-p7-NS2-NS3-NS4A-NS4B-NS5A-NS5B-COOH) through co- and posttranslational processing of the polyprotein by cellular and viral proteases (20, 36).

In Pestiviruses the p7 gene encodes for a small hydrophobic polypeptide with an apparent molecular mass of 6 to 7 kDa (7) that has been regarded as an ion channel forming protein due to its similarities to hepatitis C virus (HCV) p7 protein. Initial reports suggest that in related BVDV p7 functions as an ion channel-forming protein (13). BVDV is sensitive to amantadine (13) and BIT225 (21), known inhibitors of HCV p7 ion channel function. Thus, it is hypothesized that CSFV p7, like HCV p7 and influenza virus M2 proteins, may function as a viroporin involved in pore formation and transport of ions across cell membranes (1, 11). Although there are similarities in the general protein structure between p7 from HCV and pestiviruses, the amino acid sequence identity between the proteins is <10% (Fig. 1). HCV p7 is also a small hydrophobic protein that consists of two putative transmembrane domains and a conserved basic cytosolic loop (5). HCV p7 has been shown to be essential for virus production but not for RNA replication (18) and possesses ion channel activity *in vitro* and establishes pores in liposomes (12, 34). The functions of p7 in the CSFV cycle are unknown, including its effect on virus replication or virulence in the natural host, and its role as a membrane channel-forming protein.

In the present study it was observed that the presence of p7 is essential for *in vitro* CSFV replication. *In vivo*, partial to complete attenuation of virulence was observed when pigs were inoculated with recombinant mutants, obtained by alanine scanning mutagenesis, harboring specific three to six amino acid residue substitutions within their native p7 amino acid sequence. The biochemical characterization of CSFV p7 using model membranes revealed that this protein possesses a robust membrane channel-forming capacity. Structure-function analyses of CSFV p7 using synthetic peptides showed that the pore-forming efficiency resides in the carboxyl half of the protein.

MATERIALS AND METHODS

Viruses and cells. Swine kidney cells (SK6) (35), free of BVDV, were cultured in Dulbecco minimal essential media (DMEM; Gibco, Grand Island, NY) with 10% fetal calf serum (FCS; Atlas Biologicals, Fort Collins, CO). CSFV Brescia strain was propagated in SK6 cells and used for the construction of an infectious cDNA clone (26). Growth kinetics were assessed using primary swine macrophage cell cultures prepared as described by Zsak et al. (40). Titration of CSFV from clinical samples was performed using SK6 cells in 96-well plates (Costar, Cambridge, MA). After 4 days in culture, viral infectivity was assessed using an immunoperoxidase assay with the CSFV monoclonal antibody WH303 (MAb WH303) (6) and a Vectastain ABC kit (Vector Laboratories, Burlingame, CA). Titers were calculated according to the method of Reed and Muench

Received 2 March 2012 **Accepted** 3 April 2012
Published ahead of print 11 April 2012
Address correspondence to M. V. Borca, manuel.borca@ars.usda.gov.

doi:10.1128/JVI.00560-12

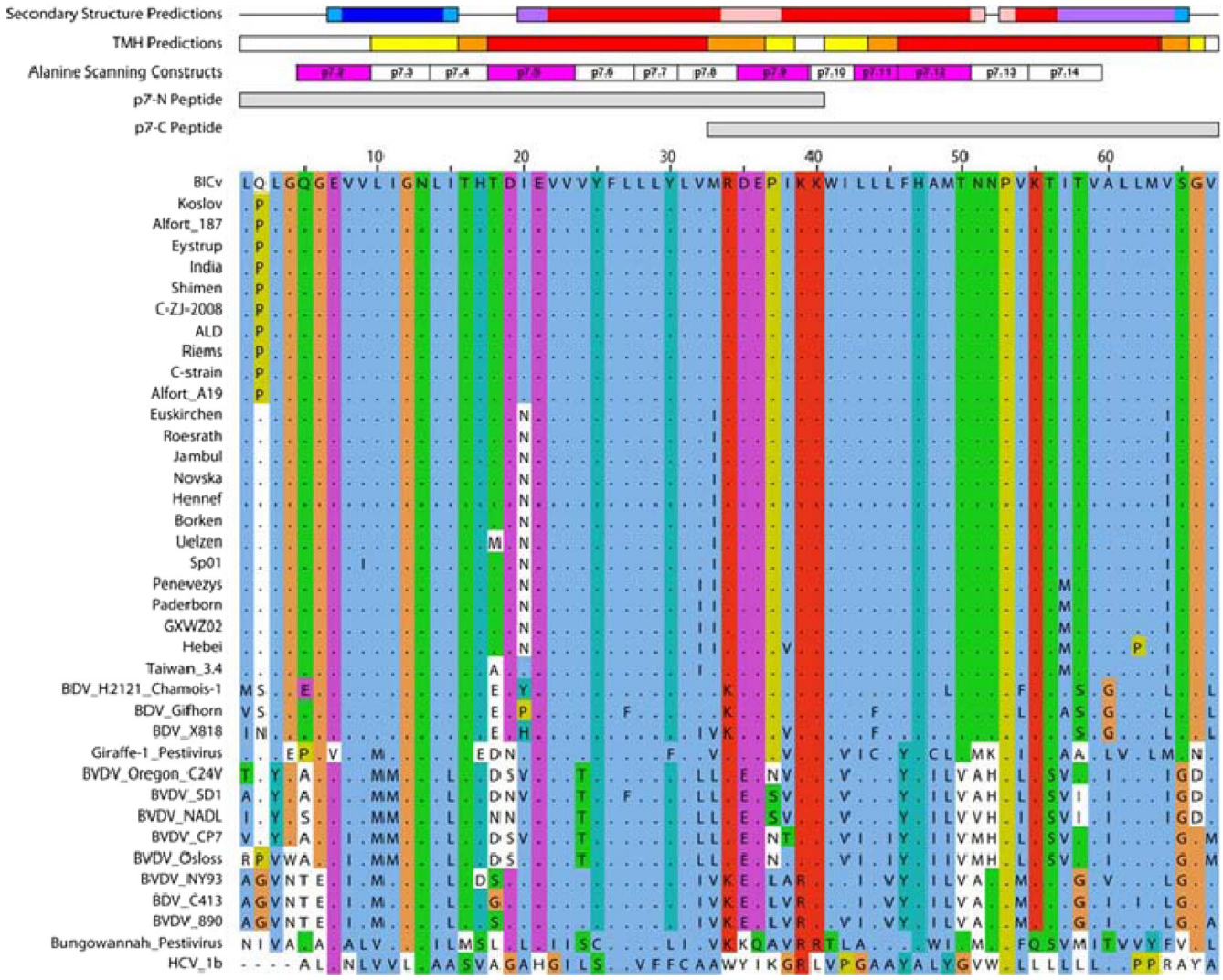

FIG 1 Annotated multiple sequence alignment of p7 homologs and predicted structural features. Residues conserved within CSFV isolates are shown as dots. The alignment is colored in the standard CLUSTAL coloring scheme. Above the multiple sequence alignment, the predicted secondary structure, the predicted transmembrane topology and alanine scanning data have been mapped to the alignment. (i) Secondary structure predictions. For areas in which PSI-PRED and SAM are in accord, helices are shown in red, strands are shown in dark blue, and coils are shown as lines. Where SAM and PSI-PRED secondary structure prediction conflict, light blue represents coil and strand predictions, light pink represents coil and helix predictions, and purple represents helix and sheet predictions. (ii) TMH predictions. A summary of the predictions from three transmembrane helix prediction algorithms—TMHMM, Spoctopus, and Memsat—is shown. Areas in which all three algorithms agree are shown in red, areas in which two agree are shown in orange, and areas in which only one algorithm predicts a TMH are shown in yellow. (iii) Alanine scanning constructs. Alanine constructs that resulted in nonviable viruses are indicated in violet.

(25) and expressed as 50% tissue culture infective dose(s) ($TCID_{50}$)/ml. The test sensitivity was $\geq \log_{10} 1.8$ $TCID_{50}$/ml.

Construction of CSFV mutants. A full-length infectious clone (IC) of the virulent Brescia strain (pBIC) (4, 26) was used as a template to obtain all cDNA IC constructs described in this report. Constructs containing in-frame partial deletions of p7 were produced using a primer mutagenesis program (Stratagene, Cedar Creek, TX). Designed constructs of p7 have deleted regions encoding amino acids 15 to 51 (p7Δ15-51), 10 to 32 (p7Δ10-32), and 33 to 51 (p7Δ33-51). IC cDNA for p7Δ15-51, p7Δ10-32, and p7Δ33-51 constructs were obtained by using the QuikChange XL site-directed mutagenesis kit (Stratagene) performed according to the manufacturer's instructions with full-length pBIC as a template. The product was then digested with DpnI, leaving only the newly amplified plasmid, transformed into XL10-Gold ultracompetent cells, and grown on Terrific broth agar plates with ampicillin (Teknova). Positive colonies were selected for by sequence analysis of the p7 gene and grown for plasmid purification using a Maxiprep kit (Qiagen Sciences, MD). Each of the IC constructs was completely sequenced to verify that only site-directed mutagenesis-induced changes were present.

A library of mutated p7 genes was developed where codons encoding for three to six residue stretches of native p7 amino acid sequence were substituted with alanine codons (Fig. 1). Full-length pBIC was used as a template in which amino acids were substituted with alanine, introduced by site-directed mutagenesis using the QuikChange XL site-directed mutagenesis kit performed according to the manufacturer's instructions in the same manner as described above for the p7 deletion constructs. Primers were designed using the Stratagene primer mutagenesis program.

***In vitro* rescue of CSFV Brescia and p7 mutants.** Full-length genomic clones were linearized with SrfI and *in vitro* transcribed using the T7 Megascript system (Ambion, Austin, TX). RNA was precipitated with LiCl and transfected into SK6 cells by electroporation at 500 V, 720 Ω, and

100 W with a 630 electroporator (BTX, San Diego, CA). Cells were seeded in 12-well plates and incubated for 4 days at 37°C in 5% CO_2. Virus was detected by immunoperoxidase staining as described above, and stocks of rescued viruses were stored at −70°C.

Amantadine and verapamil studies. SK6 cells were grown in a six-well plates up to a density of 80% confluence and treated with the indicated concentrations (see Fig. 4) of either drug for 30 min. Cells were then infected with BICv (multiplicity of infection [MOI] = 0.1) for 1 h, washed twice with phosphate-buffered saline (PBS), and then incubated in growth medium for 72 h. Viral progeny yields were determined in samples taken at 48 and 72 h postinfection. Each point represents the mean $\log_{10}$ $TCID_{50}$/ml and standard deviations from two independent experiments. The sensitivity of virus detection was $\geq\log_{10}$ 1.8 $TCID_{50}$/ml.

The toxic effect of amantadine or verapamil on treated SK6 cells was assessed with a colorimetric cell viability assay based on the reduction of MTT [3-(4,5-dimethylthiazol-2-yl)-2,5-diphenyltetrazolium bromide]. SK6 cells were treated with different concentrations of amantadine or verapamil for 72 h and then exposed to MTT (5 mg/ml in PBS) (Promega, Madison, WI) for 1 h. The reduction of MTT was determined by measuring the absorbance as the optical density at 540 nm (OD_{540}). Cell viability was determined as follows: (OD_{540} untreated/OD_{540} treated) × 100.

Western blot analysis. Expression of glycoprotein E2 by BICv and the mutant viruses was analyzed in lysates of SK6-infected cells by Western immunoblotting. CSFV E2 was detected with MAb WH303. SK6 monolayers were infected (MOI = 1) with BICv or mutants, harvested at 48 h postinoculation (hpi) using the NuPAGE LDS sample buffer system (Invitrogen), and incubated at 70°C for 10 min. Samples were run under reducing conditions in precast NuPAGE 12% bis-Tris acrylamide gels (Invitrogen). Western immunoblots were performed using the WesternBreeze chemiluminescent immunodetection system (Invitrogen).

Detection of viral RNA. Total RNA was isolated from infected SK6 cell using RNeasy (Qiagen, Valencia, CA). The real-time PCR assay was designed as a probe hydrolysis (TaqMan)/reverse transcription-PCR (RT-PCR) single-tube assay (Tetracore, Rockville, MD). Specific oligonucleotide primers and the fluorogenic probe target a highly conserved region within the 5′ untranslated region of the CSFV genome (GenBank accession number NC_000294.1). The TaqMan probe was labeled with a 5′ reporter dye, 6-carboxyfluorescein, and a 3′ quencher, 6-carboxy-*N*,*N*,*N*′,*N*′-tetramethyl rhodamine (TAMRA; PE Biosystems, Foster City, CA). RT-PCRs were performed as described by the manufacturer (Tetracore).

DNA sequencing and analysis. Full-length clones and *in vitro*-rescued viruses were completely sequenced with CSFV-specific primers by the dideoxynucleotide chain-termination method (30). Viruses recovered from infected animals were sequenced in the region of the genome that contained the desired mutations. Sequencing reactions were prepared with a dye terminator cycle sequencing kit (Applied Biosystems, Foster City, CA). Reaction products were sequenced on a Prism 3730xl automated DNA sequencer (Applied Biosystems). Sequence data were assembled using Sequencher 4.7 software (Genes Codes Corp., Ann Arbor, MI). The final DNA consensus sequence represented, on average, a 3- or 4-fold redundancy at each base position.

Animal infections. Virulence of p7 mutant viruses relative to BICv was initially assessed in 10 to 12 weeks old, forty-pound commercial-breed pigs inoculated intranasally (i.n.) with 10^5 $TCID_{50}$ of each virus. Pigs were randomly allocated into nine groups of four animals each and were inoculated with a p7 virus mutant or BICv. Clinical signs (anorexia, depression, purple skin discoloration, staggering gait, diarrhea, and cough) and changes in body temperature were recorded daily throughout the experiment and scored as previously described (23). Blood was collected at various times postinfection from the anterior vena cava into EDTA-containing tubes (Vacutainer) for total and differential white blood cell counts (performed using a Beckman Coulter ACT [Beckman Coulter, CA]) and quantification of viremia by virus titration as described above.

For infection-challenge studies, 12 pigs were randomly allocated into two groups containing five animals each and a third group containing two animals. Pigs in groups 1 and 2 were i.n. inoculated with 10^5 $TCID_{50}$ of p7.10 virus, and pigs in group 3 were mock infected. At 3 days postinoculation (dpi) (group 1) or 28 dpi (group 2), animals were challenged with 10^5 $TCID_{50}$ of BICv along with animals in group 3. Clinical signs and body temperature were recorded daily throughout the experiment as described above. Blood samples were collected at times postchallenge for blood cell counts and quantification of viremia as described previously.

TABLE 1 Detection of viral genomic RNA using real-time RT-PCR in extracts from SK6 cells transfected with p7 mutant constructs that do not yield viral progeny

p7 mutant RNA construct	C_T value	Viral RNA detection
p7.2	21.53	+
p7.5	21.98	+
p7.9	17.97	+
p7.11	18.35	+
p7.12	22.98	+
p7Δ10-32	16.41	+
p7Δ15-51	0.00	–
p7Δ35-51	0.00	–
BICv	20.71	+

Synthetic peptides. The CSFV p7 Brescia strain protein and its derived p7-N and p7-C peptides (sequences displayed in Fig. 1) were commercially synthesized (Thermo Scientific). The purified peptides were dissolved in dimethyl sulfoxide (DMSO; spectroscopy grade), and their concentrations were determined by bicinchoninic acid microassay (Pierce, Rockford, IL). Small, diluted aliquots (typically, 20 μl [1 mg/ml]) were stored frozen and were thawed only once, upon use.

CD studies. Circular dichroism (CD) measurements were obtained from a thermally controlled Jasco J-810 CD spectropolarimeter calibrated routinely with (1*S*)-(+)-10-camphorsulfonic acid, ammonium salt. Samples consisted of lyophilized peptides dissolved at concentrations of 0.03 mM in 2 mM HEPES (pH 7.4) buffer containing 50% 1,1,1,3,3,3-hexafluoro-2-propanol (HFIP). Spectra were measured in a 1-mm pathlength quartz cell initially equilibrated at 25°C. The data were taken with a 1-nm bandwidth at 100 nm/min speed, and the results of 20 scans were averaged.

Pore formation in lipid vesicles. Large unilamellar vesicle(s) (LUV) were prepared according to the extrusion method (15). Phosphatidylcholine (PC), phosphatidylethanolamine (PE), phosphatidylglycerol (PG), phosphatidylinositol (PI), and phosphatidylserine (PS) were purchased from Avanti-Polar Lipids (Birmingham, AL). The 8-aminonaphthalene-1,3,6-trisulfonic acid sodium salt (ANTS) and *p*-xylenebis(pyridinium) bromide (DPX) were obtained from Molecular Probes (Junction City, OR). Lipid mixtures in organic solvent were dried under an N_2 stream. Traces of organic solvent were removed by vacuum pumping. Subsequently, dried lipid films were dispersed in buffer and subjected to 10 freeze-thaw cycles before extruding them 10 times through two stacked polycarbonate membranes with a nominal pore size of 0.1 μm (Nuclepore, Inc., Pleasanton, CA). Vesicle permeabilization was assayed by monitoring the release to the medium of encapsulated fluorescent ANTS (ANTS-DPX assay) (8). LUV containing 12.5 mM ANTS, 45 mM DPX, 20 mM NaCl, and 5 mM HEPES were obtained by separating the unencapsulated material by gel-filtration in a Sephadex G-75 column that was eluted with 5 mM HEPES and 100 mM NaCl (pH 7.4). Internal and external osmolarities were measured in a cryoscopic osmometer (Osmomat 030; Gonotec, Berlin, Germany) and adjusted by adding NaCl. Fluorescence measurements (intensity versus time) were performed in an SLM Aminco 8100 spectrofluorimeter (Spectronic Instruments, Rochester, NY) by setting the ANTS emission at 520 nm and the excitation at 355 nm. A cutoff filter (470 nm) was placed between the sample and the emission monochromator. The baseline leakage (0%) corresponded to the fluores-

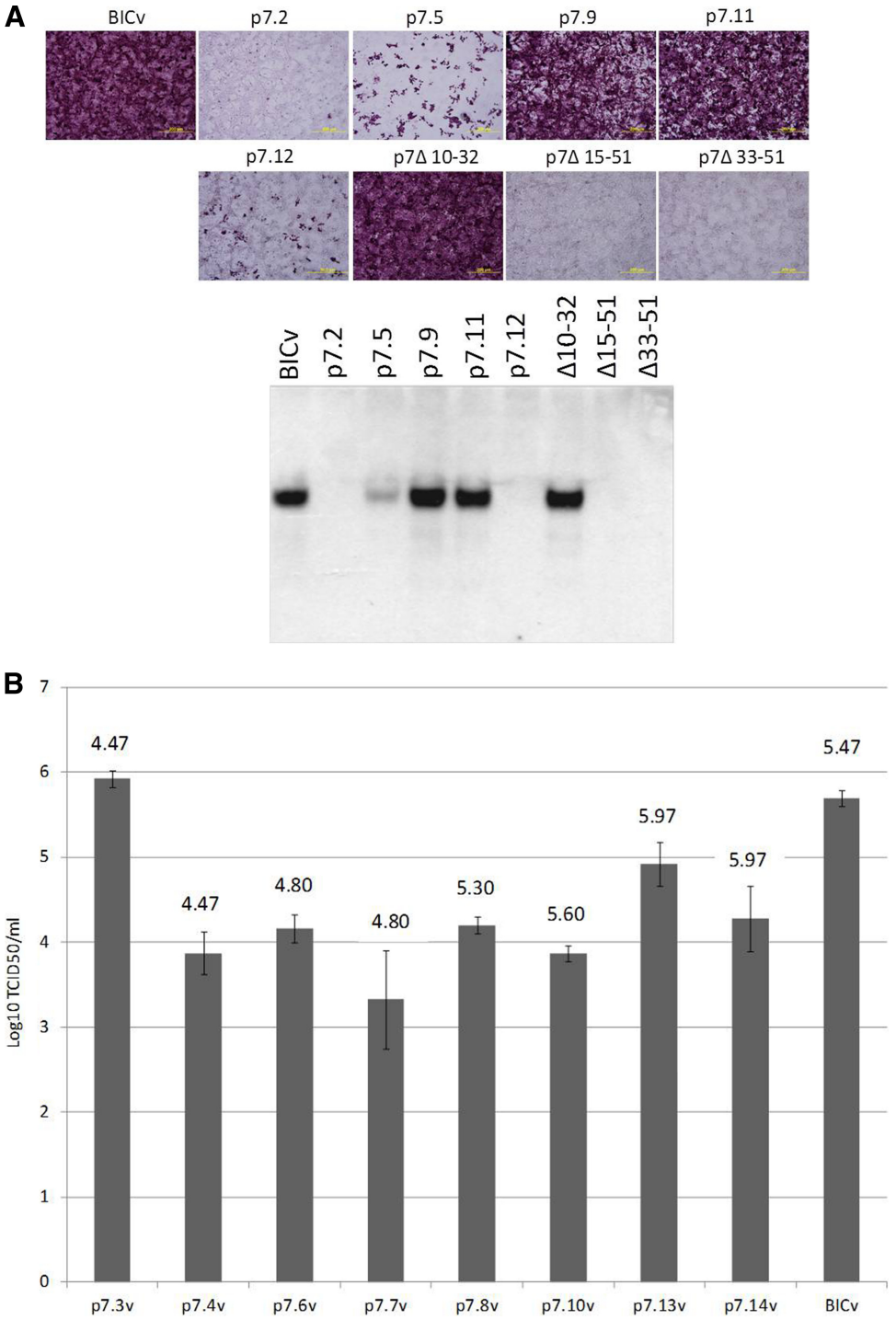

FIG 2 Virus protein expression after transfection and *in vitro* growth characteristics of p7 mutants and parental BICv. (A) Detection of CSFV E2 protein by immunocytochemistry (top panel) and Western blotting (bottom panel) in SK6 cells transfected with recombinant construct that do not yield virus progeny. (B) Primary swine macrophage cell cultures were infected (MOI = 0.01) with each of the mutants or parental BICv, and the virus yield was titrated at 72 h postinfection in SK6 cells. The data represent means and standard deviations from two independent experiments. The sensitivity of virus detection was $\geq \log_{10} 1.8$ $TCID_{50}$/ml. Values shown above the bars represent the virus yield ($\log_{10}$ $TCID_{50}$) detected 4 days after transfection of SK6 cells with the corresponding *in vitro*-transcribed RNA.

cence of the vesicles at time zero, while 100% leakage was the fluorescence value obtained after addition of Triton X-100 (0.5% [vol/vol]).

Bioinformatic and structural predictions. Secondary structure predictions were made by SAM and PSI-PRED (19, 22). Transmembrane helix topology predictions were made using TMHMM, Memsat, and Spoctopus (22, 31, 39). Tertiary predictions were performed using RosettaMembrane (2). Multiple folding trajectories were performed for CSFV p7 of the Brescia strain (BICv), and homologs and the resulting models were clustered with the lowest energy BICv p7 member of the largest cluster selected for further analysis.

RESULTS

Comparison of CSFV p7 amino acid sequence with those of other pestiviruses and HCV. CSFV p7 is a small hydrophobic protein comprised of 67 amino acid residues. Comparison of its amino acid sequence among different CSFV isolates reveals more than 89.5% identity among isolates (Fig. 1). Compared to other pestiviruses, the amino acid identity ranges between 50 and 55% relative to BVDV isolates and between 50 to 70% relative to BDV isolates. The protein homolog in HCV is also a small hydrophobic protein, although amino acid identities between CSFV and HCV p7 proteins are typically <10%. HCV p7 largely comprises of two predicted transmembrane alpha helices joined through a fully conserved basic loop (Fig. 1). Despite a low degree of amino acid sequence identity, CSFV p7 presents a general structure similar to that of HCV p7.

p7 is essential for CSFV production. To assess the importance of the integrity of p7 in the development of infectious particles, infectious clone cDNA constructs containing in-frame partial deletions of p7 were designed in the context of a full-length cDNA clone of CSFV Brescia strain (26). Three different in-frame partial deletions were designed involving central areas of p7 (Δ10-32, Δ15-51, and Δ33-51), while leaving the possible cleavage sites on both ends of the protein unaltered (residues 1 to 9 and residues 52 to 67, respectively). Infectious RNA was *in vitro* transcribed from each of the cDNA constructs and was subsequently used to transfect SK6 cells. Transfections using any of these p7 partial deletion constructs were invariably negative (after three independent events) in terms of recovering infectious particles (data not shown).

Construction of CSF p7 mutant viruses. To assess the importance of p7 for virus production, a series of recombinant CSFVs containing mutations in p7 were designed using the cDNA infectious clone of the Brescia strain (BICv) as a template. A total of 14 cDNA constructs containing sequential areas of three to six amino acid residues in the native p7 amino acid sequence substituted by alanine residues were constructed (Fig. 1). Infectious RNA was *in vitro* transcribed from each mutated full-length cDNA and used to transfect SK6 cells. Infectious virus was rescued from transfected cells by day 4 posttransfection using constructs p7.3, p7.4, p7.6, p7.7, p7.8, p7.10, p7.13, and p7.14 (depicted as white blocks in Fig. 1). In contrast, after three independent transfection procedures, p7.2, p7.5, p7.9, p7.11, and p7.12 constructs did not produce infectious viruses (depicted as violet blocks in Fig. 1). Real-time RT-PCR analysis of total RNA extracted from these cells and cells transfected with p7Δ10-32, p7Δ15-51, and p7Δ33-51 constructs revealed genomic RNA replication, except for the p7Δ15-51 and p7Δ33-51 constructs (Table 1). In addition, immunohistochemistry and Western blot analysis (Fig. 2A) of transfected cell extracts showed comparable results showing a differential expression of structural glycoprotein E2. As expected, p7Δ15-51 and p7Δ33-51 failed to produce any detectable levels of E2. p7.2-transfected cells present a very low level of expression of E2 only detectable by immunocytochemistry, whereas the levels of E2 in p7.5- and p7.12-transfected cells are intermediate relative to the levels observed in p7.9, p7.11, p7Δ10-32, and BICv cell extracts. Partial nucleotide sequencing of the rescued p7 mutated viruses was performed to ensure the presence of the predicted mutations.

Growth of the CSFV p7 mutants *in vitro*. *In vitro* growth characteristics of the p7 mutant viruses relative to parental BICv were evaluated in a single-step growth curve. Primary swine macrophage cell cultures were infected at an MOI of 0.01 $TCID_{50}$ per cell. Viruses were adsorbed for 1 h (time zero), and samples were collected at 72 h postinfection and titrated in SK6 cell cultures. With the exception of p7.3v, all mutant viruses exhibited a reduction (between 1 to 2.5 $\log_{10}$, depending on the virus considered) in their virus titers compared to that of the parental BICv (Fig. 2). This reduction varies among the mutants, being most drastic for viruses p7.4, p7.7, and p7.10. Each exhibited a reduction in their titers by approximately 2 to 2.5 $\log_{10}$ compared to the parental BICv.

Virulence of CSFV p7 mutants *in vivo*. To examine whether alterations of different regions of p7 affect virulence, different groups of pigs were i.n. inoculated with ~10^5 $TCID_{50}$ of each of the p7 mutant viruses (p7.3, p7.4, p7.6, p7.7, p7.8, p7.10, p7.13, and p7.14) and monitored for clinical disease, evaluated relative to parental BICv (Table 2). All animals infected with BICv presented clinical signs of CSF starting 3 to 5 dpi, developing classical symptoms of the disease and dying around 11 to 12 dpi. Total white blood cells, lymphocytes, and platelet counts dropped by 4 to 6 dpi in animals inoculated with BICv and continued declining until death (Fig. 3A, B, and C). Viruses p7.3, p7.6, p7.7, and p7.13 presented a virulence phenotype almost indistinguishable from that of the parental BICv (Table 1). All animals infected with these viruses presented clinical signs of CSF starting at 4 to 5 dpi, with clinical presentation and severity similar to those observed in animals inoculated with BICv. White blood cells, lymphocytes, and platelet counts dropped by 4 dpi and continued declining until death (Fig. 3A, B, and C) at 11 to 14 dpi. Animals infected with viruses p7.4 or p7.8 presented a transient (during 2 and 5 days, respectively) rise in body temperature accompanied by mild depression and anorexia, returning to clinical norms by 9 to 10 dpi (Table 2). A drop in lymphocytes and platelet counts was also transient accompanying the presence of clinical signs (Fig. 3A, B, and C). Animals inoculated with p7.14 virus presented disease-related symptoms by 5 dpi. Interestingly, disease progressed in one of the animals dying at 11 dpi, while the others clinically recuperated after a 2- to 4-day period of transient rise in body temperature, depression, and anorexia (Table 2). White blood cells, lymphocytes, and platelet counts decreased in all animals in this group, remaining low in the animal dying at 11 dpi and reaching intermediate values in the surviving animals by the end of the

TABLE 2 Swine survival and fever response after infection with p7 CSFV mutant viruses and parental BICv

Virus	No. of survivors (n = 4/virus)	Mean time to death (days ± SD)	Fever (days ± SD)	
			Time to onset	Duration
p7.3	0	13.67 ± 3.51	5 ± 0	9.32 ± 3.06
p7.4	4		5 ± 0	2 ± 0
p7.6	0	11.34 ± 4.95	5.5 ± 0.58	5.5 ± 4.95
p7.7	0	14 ± 0	5.67 ± 0	5 ± 0
p7.8	4		2 ± 1.72	5.67 ± 0.58
p7.10	4			
p7.13	0	12.67 ± 3.79	4 ± 0	7.32 ± 1.52
p7.14	3	11[a]	5 ± 0	3 ± 2.65
BICv	0	11.25 ± 0.96	3.75 ± 0.5	6.75 ± 0.96

[a] The data here correspond to the only animal that did not survive the infection.

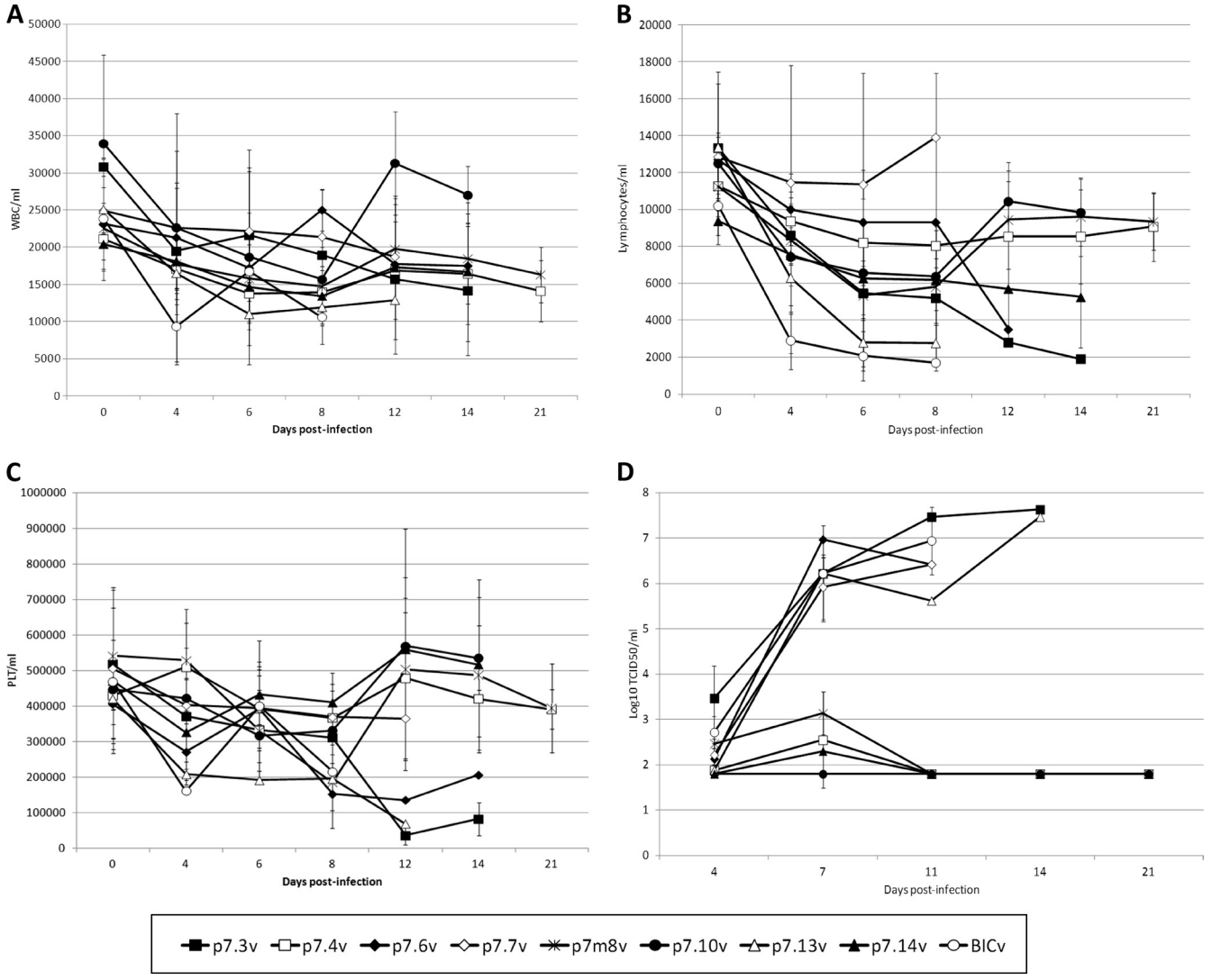

FIG 3 Hematologic changes (A, B, and C) and viremia titers (D) detected in pigs inoculated with p7 mutant viruses or parental BICv. Animals were intranasally infected with 10^5 $TCID_{50}$ of each of the p7 mutant viruses or BICv. Each point represents the mean log_{10} $TCID_{50}$/ml and standard deviations from at least three animals. The sensitivity of virus detection was $\geq log_{10}$ 1.8 $TCID_{50}$/ml. White blood cell (WBC [A]), lymphocyte (lymph [B]), and platelet (PLT [C]) counts were determined during the infection.

experimental period (Fig. 3A, B, and C). Finally, animals inoculated with virus p7.10 survived the infection and remained clinically normal throughout the observation period (21 days). In these animals there was a transient decrease in all of the hematological values by 6 dpi, with values returning to normal by 12 dpi (Table 2 and Fig. 3A).

Viremia in animals inoculated with p7 mutants varied and in general accompanied the evolution of the clinical disease (Fig. 3D). Animals inoculated with virulent viruses p7.3, p7.6, p7.7, or p7.13 exhibited viremia kinetics almost undistinguishable from that induced by parental BIC virus, presenting high titers that remained until death of the animal. Viruses p7.4, p7.8, and p7.14 induced a mild disease and transient viremia, with virus titers significantly lower than those found in animals inoculated with parental BIC virus. Finally, no virus could be detected at any sample point in blood from animals infected with the p7.10 virus,

TABLE 3 Swine survival, fever response, and viremia in pigs infected with p7.10v and challenged with parental BICv

Challenge, time administered	No. of survivors/ total no.	Mean time to death (days ± SD)	Fever (days ± SD)		Viremia (avg titer at 5 dpc ($TCID_{50}$/ml ± SD)
			Time to onset	Duration	
p7.10v, 3 dpi	3/5	11 ± 1.41; –[a]	3.2 ± 0.45; 3 ± 0[a]	7.5 ± 1.41; 2.67 ± 0.58[a]	5.89 ± 1.2; 2.85 ± 0.95[a]
p7.10v, 28 dpi	5/5				≤1.8
Mock	0/2	10 ± 2.12	3.5 ± 1.41	7.5 ± 0.71	5.97

[a] The first value corresponds to the two animals that did not survive challenge; the second value corresponds to the three animals that survived challenge.

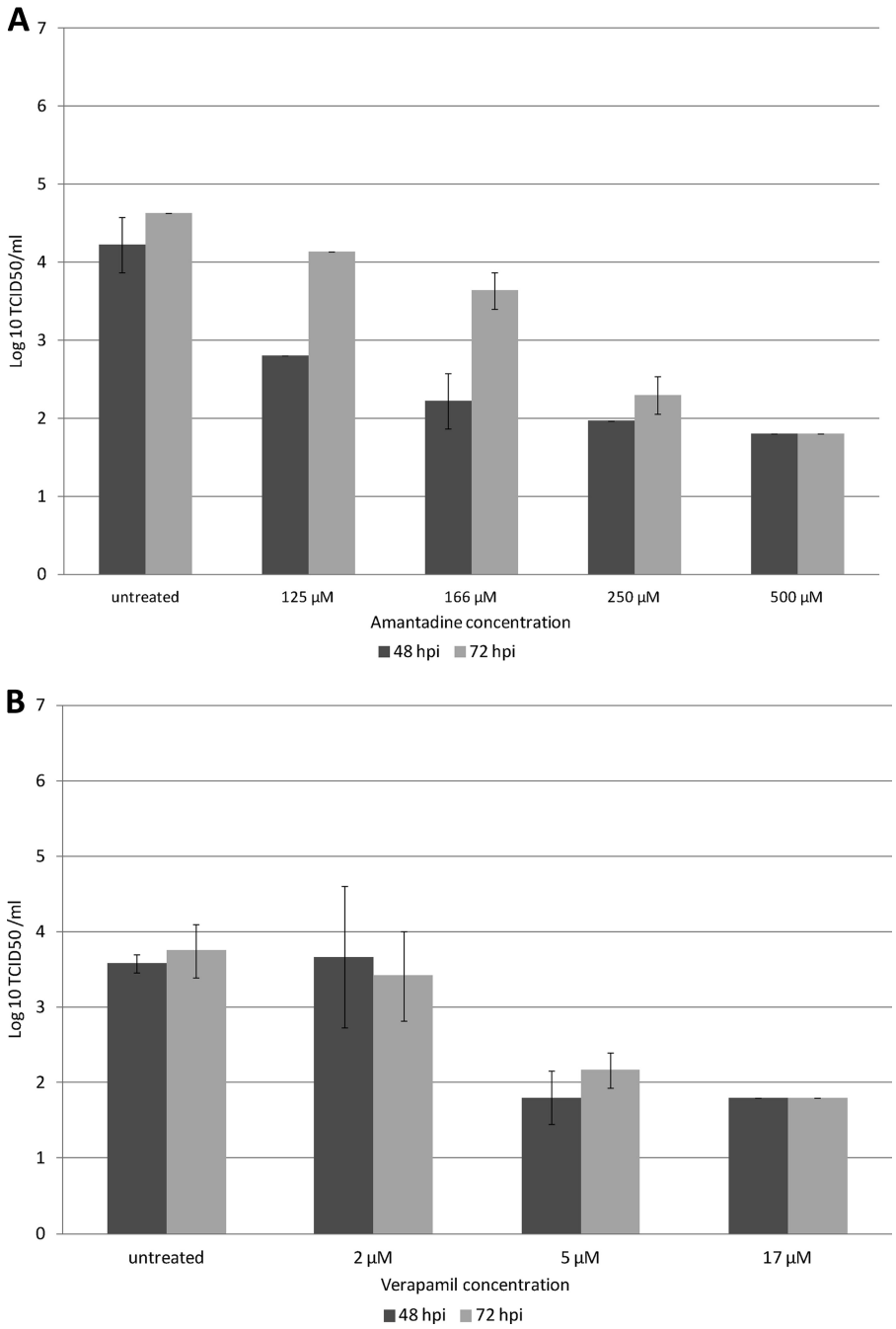

FIG 4 Effect of amantadine (A) and verapamil (B) treatment on SK6 cell cultures infected with CSFV. SK6 cell cultures were treated with either drug for 30 min and then infected with BICv (MOI = 0.01), and the virus yield was assessed at 48 and 72 h postinfection. Each point represents the mean $\log_{10}$ $TCID_{50}$/ml and standard deviations from two independent experiments. The sensitivity of virus detection was $\geq\log_{10}$ 1.8 $TCID_{50}$/ml.

indicating that this virus developed a very mild infection when inoculated i.n.

p7.10 mutant virus infection protects pigs against lethal CSFV challenge. The limited *in vivo* replication kinetics of p7.10 virus is similar to that observed with CSICv, a CSFV vaccine strain (26). However, restricted *in vivo* replication could also impair protection against wild-type virus infection. Thus, the ability of p7.10 virus to induce protection against virulent BICv was assessed in early and late vaccination-exposure experiments. Groups of pigs ($n = 5$) were i.n. inoculated with 10^5 $TCID_{50}$ of p7.10 virus and i.n. challenged with 10^5 $TCID_{50}$ of parental BICv at either 3 or 28 dpi. Mock-vaccinated control pigs receiving BICv only ($n = 2$) developed anorexia, depression, and fever by 4 days postchallenge (dpc), as well as a marked reduction in circulating total leukocytes, lymphocytes, and platelets by 4 dpc (data not shown), and died or were euthanized *in extremis* by 10 dpc after showing high viremia titers since dpc 4 (Table 3). Animals challenged at 3 dpi presented a heterogeneous behavior: two of them showed a clinical disease,

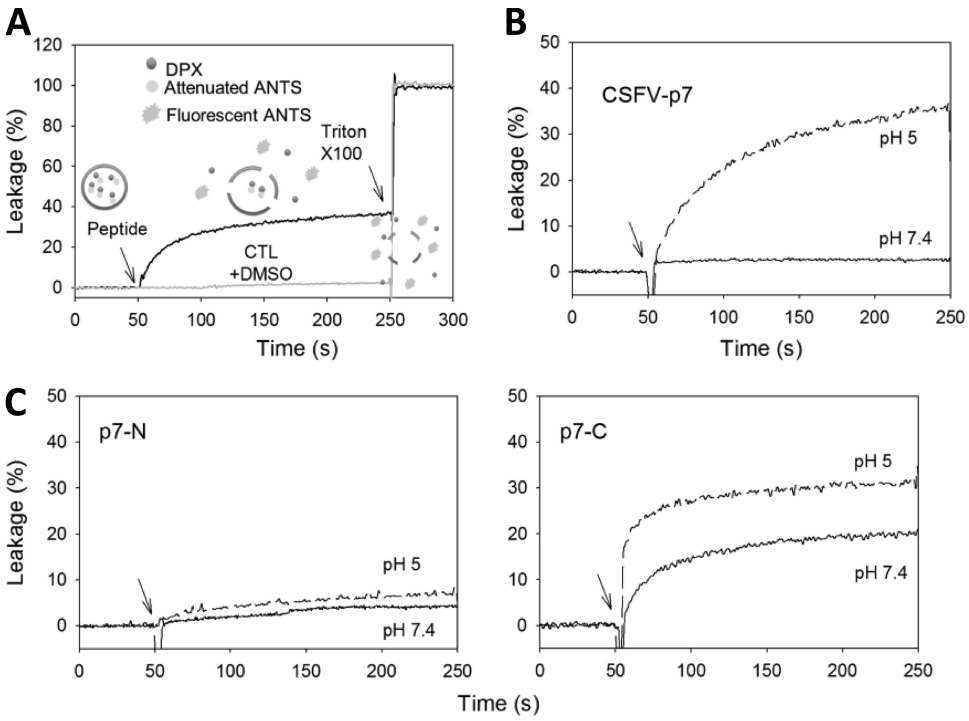

FIG 5 Pore-forming activity of BICv p7 protein and derived peptides as detected by the ANTS-DPX assay. (A) Schematics of the ANTS-DPX assay (see the text for the explanation). (B) Permeabilization induced by BICv p7 protein of large unilamellar vesicles composed of the main ER phospholipids PC-PE-PI (5:3:2 molar ratio). Leakage of vesicular internal aqueous contents is shown as a function of time. At the time indicated by the arrow, the protein was injected into a stirring cuvette. The protein/lipid molar ratio was 1:100. The lipid concentration was 100 μM. (C) Permeabilization induced by p7-N and p7-C (left and right panels, respectively) of ER LUV. Conditions were as described in the previous panel. Assays were performed at pH 7.4 or 5.0 as indicated in the panels.

hematological values, and viremia titers indistinguishable from mock-vaccinated animals (Table 3). Conversely, the other three animals in the group became clinically and hematologically normal after a transient disease by 5 dpc (Table 3). Infection with p7.10 virus induced complete protection by 28 dpi. All pigs survived the BICv challenge and remained clinically normal (Table 3) without significant changes in their hematological values (data not shown). Thus, even though p7.10 virus exhibited a limited *in vivo* growth, a solid protection was induced after vaccination.

Effect of treatment with amantadine or verapamil in cell cultures infected with CSFV. As demonstrated earlier, the integrity of p7 is critical to the process of CSFV replication. To gain insight into the possible mechanism mediating this role, the effects of amantadine and verapamil on CSFV replication were evaluated. These drugs have both demonstrated the ability to inhibit membrane permeation induced by HCV p7 viroporin (12, 13, 34). The effect of both drugs on the replication of BICv was analyzed using SK6 cell cultures. SK6 cell cultures were pretreated with 125 to 500 μM amantadine or 2 to 17 μM verapamil or were mock treated for 30 min before infection with BICv. The cells were incubated with CSFV Brescia strain at an MOI of 0.01 for 1 h at 37°C, washed with PBS, and incubated at 37°C in DMEM–10% FCS. Samples were taken for virus titration at 48 and 72 h. Treatment with either drug effectively decreased virus yields. Using the highest concentration of either drug produced an ~100-fold reduction in virus yield compared to the mock-treated cultures (Fig. 4).

In addition, it was determined that amantadine and verapamil had no significant cytotoxic effect on SK6 cells at the concentration used here. Toxicity was determined by reduction of MTT by SK6 cells exposed to these drugs for 72 h. The results showed that cells treated with amantadine (500 μM) or verapamil (17 μM) presented viabilities of 105% ± 10.7% and 87.02% ± 3.1%, respectively, relative to mock-treated cells. These results clearly indicate that the decrease in virus titers observed is not due to a cytotoxic effect mediated by these drugs.

Pore-forming activity and structural characterization of CSFV p7 and derived peptides p7-N and p7-C. Structure-function analyses of CSFV p7 as a prospective viroporin were next carried out using the synthetic BICv p7 protein sequence and its derived peptides, p7-N and p7-C. As displayed in the top diagrams of Fig. 1, p7-N and p7-C sequences spanned the potential N- and C-terminal transmembrane regions of BICv p7, respectively, and overlapped along the conserved polar loop sequence.

CSFV p7 is predicted to insert into the endoplasmic reticulum (ER) membrane (20). Therefore, the pore-forming activity of these synthetic sequences was assessed in lipid vesicles that emulated the ER membrane (Fig. 5). The lipid bilayer surrounding this organelle is essentially symmetric (both monolayers with equal lipid composition) and mostly devoid of sterols (37). Thus, the lipid composition of the liposomes was based on the main constituent phospholipids of the ER membrane, namely, zwitterionic PC and PE plus the anionic PI mixed in a roughly 5:3:2 molar ratio (37).

Permeabilization to low-molecular-weight markers was monitored by the ANTS-DPX assay (8, 17), which is based on the quenching of 8-aminonaphthalene-1,3,6-trisulfonic acid disodium salt (ANTS; molecular weight, 427) fluorescence by *p*-xylenebis

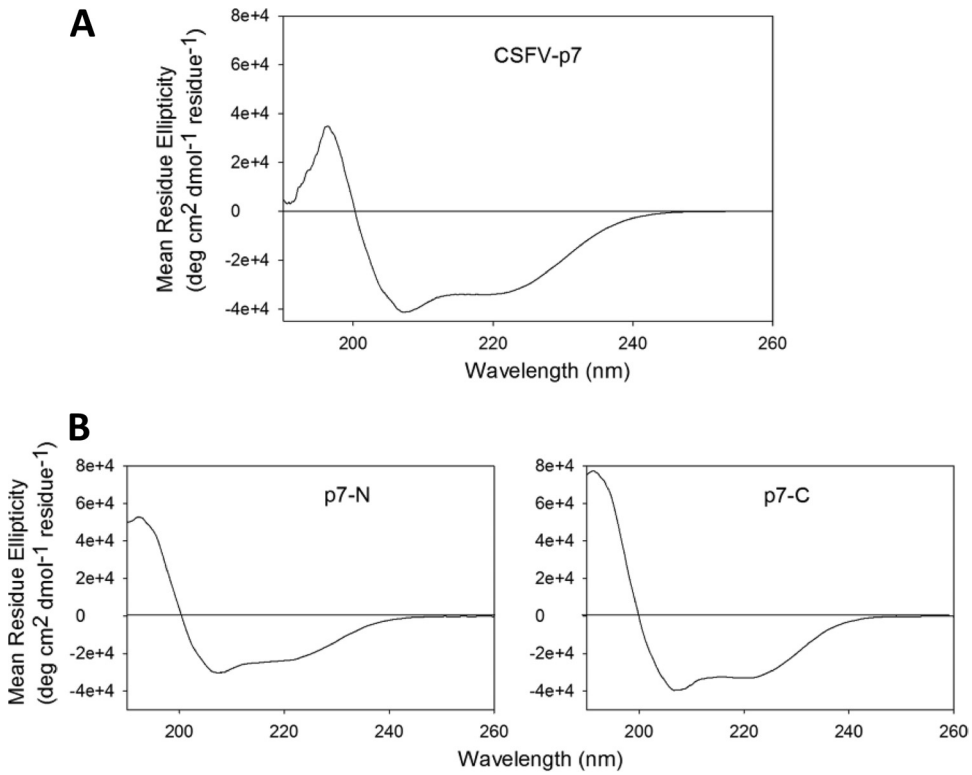

FIG 6 Structure of BICv p7 protein and derived peptides in 50% HFIP membrane-mimetic. (A) CD spectrum of BICv p7. (B) CD spectra of p7-N (left) and p7-C (right) peptides.

(pyridinium)bromide (DPX; molecular weight, 422). ANTS and DPX are true markers of the aqueous space of the liposomes and, when coencapsulated, DPX efficiently quenches ANTS fluorescence by collisional transfer (Fig. 5A). In addition, highly soluble ANTS and DPX remain trapped for extended periods, as reflected by the stability of the ANTS signal in negative-control samples treated with DMSO (Fig. 5A, CTL, gray trace), and allow permeability measurements at acidic pH (8). Upon addition of the permeabilizing agent (indicated by the arrow in Fig. 5A), both probes are released to the medium through membrane-permeating pores. Dilution of DPX prevents quenching outside the liposomes, and membrane permeabilization can be monitored as a function of time from the recovery of ANTS fluorescence (Fig. 5A, black trace). Maximal attainable ANTS fluorescence in the mixture (100% release) can be inferred after detergent solubilization of liposomes (indicated by the second arrow). In a typical experiment, 10 μl of peptide dissolved in DMSO was injected into a fluorimeter cell containing 1 ml of a stirring solution of liposomes. Previous works demonstrate that this experimental setup ensures fast and efficient partitioning of peptides into membrane surfaces (17).

The data displayed in Fig. 5B demonstrate that the complete p7 CSFV can efficiently permeabilize ER liposomes at pH 5.0 but not at pH 7.4. The lack of activity at neutral pH was probably due to limited solubility of the protein under those conditions (not shown). Liposome permeabilization and its elicitation at the lower pH could be reproduced by the p7-C peptide, but barely by the p7-N peptide (Fig. 5C, right and left panels, respectively). This observation would be consistent with a pore-forming activity residing in the carboxyl half of the protein represented by the p7-C peptide.

To test whether BICv-p7 could adopt a defined secondary structure in the nonpolar membrane medium, the synthetic sequences were next characterized by CD (Fig. 6). Consistent with their potential for adopting main α-helical conformations in nonpolar medium, the complete protein and the p7-N and p7-C peptides dissolved in 50% HFIP displayed spectra with absorption maximum located at 195 nm and minima at 208 and 222 nm (Fig. 6A and B, respectively). Deconvolution of these spectra using the CDPro software package (32) suggested a higher amount of helical conformers in p7-C than in p7-N. In contrast, this latter peptide disclosed a higher content of turns and disordered structures. Thus, the structural data support the capacity of the BICv-p7 hydrophobic domains for spanning lipid bilayers as transmembrane helices and suggest a higher conformational plasticity for the N-terminal sequence not bearing the pore-forming activity.

To further study the physiological relevance of the pore-forming activity of the p7-C sequence, we next characterized the lipid dependence of this phenomenon (Fig. 7 and 8) and the capacity of amantadine and verapamil for inhibiting the process (Fig. 9). The kinetic traces displayed in Fig. 7A demonstrate a PI-dependent pore-forming p7-C activity in vesicles emulating the ER membrane (right panel), which could not be detected in the case of p7-N (left panel). The permeabilization data also indicate that pore-formation by p7-C was even more efficient when PI was mixed with PC or PE. The data in Fig. 7B further show that anionic PS, a minor component of the ER membrane, could not substitute for PI. Interestingly, PG, an anionic phospholipid mostly present in bacterial membranes and mitochondria, could sustain p7-C

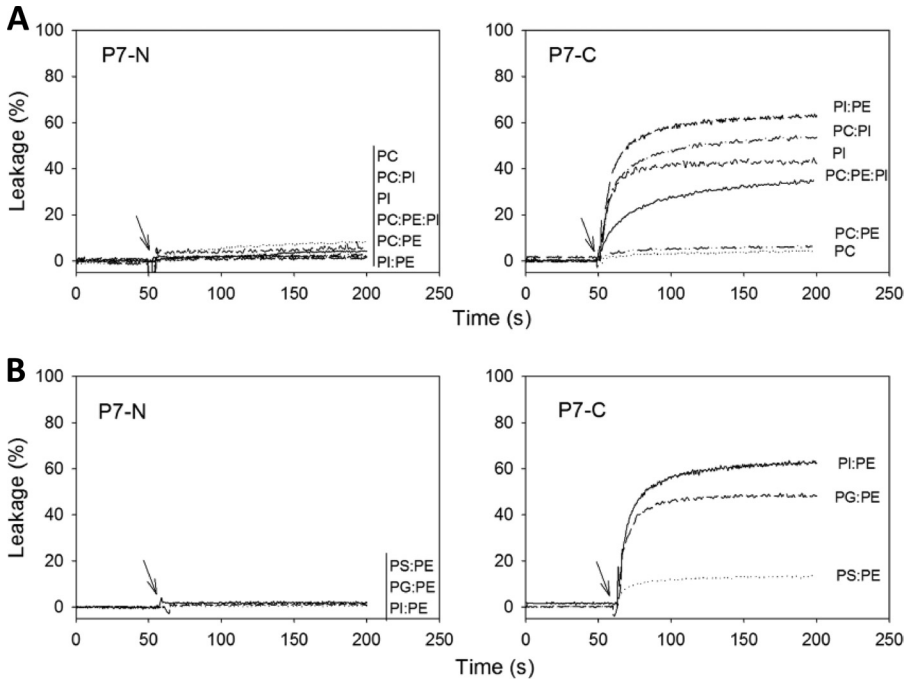

FIG 7 Effects of lipid composition on pore formation. (A) Permeabilization was induced by p7-N and p7-C (left and right panels, respectively) of large unilamellar vesicles composed of the main ER phospholipids mixed as follows: PC-PE-PI (5:3:2 molar ratio), PI-PE (1:1); PC-PI (1:1), PC-PE (1:1), PC alone, and PI alone. The peptide/lipid molar ratio was 1:50. The lipid concentration was 100 μM. (B) Permeabilization of vesicles made of equimolar mixtures of PE and anionic phospholipids. Conditions were as described in panel A.

pore-forming activity alone (data not shown) or upon mixing it with PE (Fig. 7B, right panel).

The dose dependency of p7-C-induced ER vesicle permeabilization is presented in Fig. 8. Both initial rates (proportional to the time required for the assembly of each pore) and final extents at the time of detergent addition (proportional to the total number of pores in the vesicle population) increased upon peptide dose increase (Fig. 8, left panel). Hence, both parameters, as inferred from this type of curve, reflected the capacity of p7-C peptide for efficient pore formation in the ER-mimicking lipid mixture (Fig. 8, right panel). Again, by comparison, p7-N activity could be barely detected under the same experimental conditions.

Contribution of the different ER mixture lipids to p7-C pore-forming efficiency was next evaluated (Fig. 8B to G). PE could not be tested in isolation because its nonlamellar nature precluded lipid bilayer formation when dispersed in buffer at pH 7.4. PC-based vesicles did not sustain pore formation (Fig. 8B). In contrast, pores were efficiently formed in vesicles made of pure PI (Fig. 8C). The probability of pore formation, but not the rate, increased when PI was mixed with PC (Fig. 8D). Moreover, compared to PI alone or a PC-PI mixture, pore-forming activity was maximal for the PI-PE mixture (Fig. 8E). This stimulatory effect of PE suggests that pore-opening may be regulated by bilayer structural properties such as spontaneous curvature or thickness, a common trend described for pore-forming proteins and channels (24). Finally, the data displayed in F and G panels demonstrate that PG, but not PS, could substitute for PI. Thus, although required, a negative net charge is not sufficient to sustain pore-forming activity, which appears to be also regulated by the chemical nature of the polar-head group moiety. Together, these data suggest that the C-terminal CSFV p7 hydrophobic domain is endowed with the capacity for effectively permeabilizing the ER membrane upon insertion.

The data displayed in Fig. 9 further demonstrate that p7-C pores can be inhibited by amantadine and verapamil (Fig. 9A and B, respectively). Preincubation with these compounds inhibited in a dose-dependent manner both the initial permeabilization rates and the final extents (right panels). Notably, in the liposome permeabilization assays verapamil was roughly an order of magnitude more potent than amantadine, following the same inhibitory pattern that was observed in the previously described viral replication assays (Fig. 4). In conjunction, the cell and liposome results suggest that pore formation by p7 constitutes a crucial event for the efficient replication of CSFV in cells.

Proposed model for CSFV p7. Secondary structure prediction algorithms predict a strand centered on residues Val8-Leu14 and two helices centered on residues Val22-Met33 and Ile38-Thr56 for BICv p7 (Fig. 1). The latter helix is predicted to have a disruption centered on residue Pro53. Transmembrane helix topology prediction algorithms predict two transmembrane helices centered on residues 18 to 32 and residues 46 to 63. Tertiary structure predictions place Glu21, His47, and Pro53 in close proximity to each other near the center of the membrane (Fig. 10). Gly12 and Asn13 are predicted to be at the luminal end of the first transmembrane helix; however, there is strong disagreement in the tertiary structure predictions surrounding these residues. The region from Arg34 to Lys40 is predicted to form a cytosolic loop by transmembrane helix and tertiary structure prediction algorithms.

DISCUSSION

This report focuses on the study of CSFV p7, a previously uncharacterized protein, to further understand its function in the process of

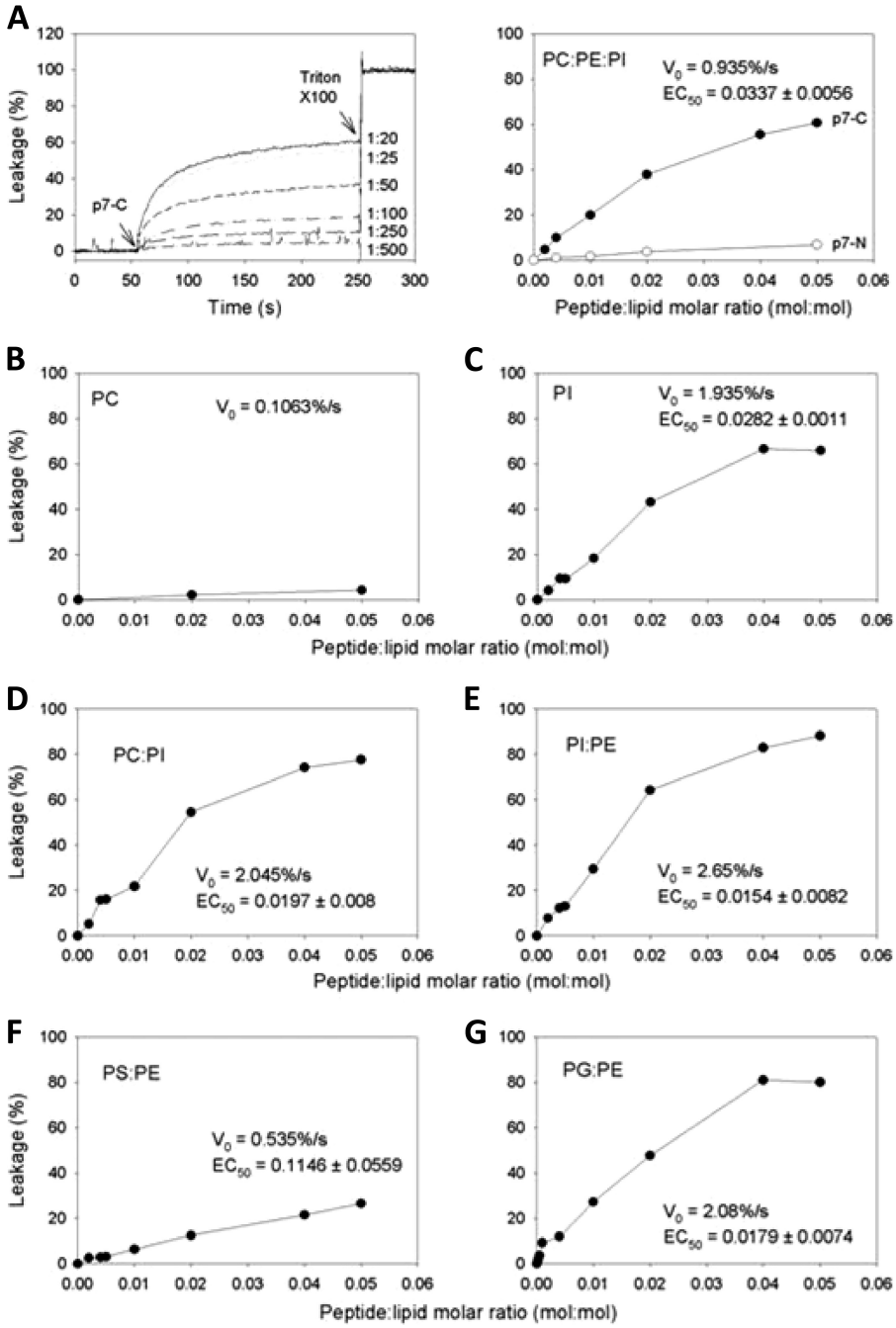

FIG 8 Contribution of the different ER mixture lipids to pore-forming efficiency. (A) The left panel shows the dose dependency of p7-C-induced permeabilization of PC-PE-PI (5:3:2) vesicles. The peptide/lipid molar ratios are indicated for each kinetic trace. The right panel shows the percentage of maximum leakage (measured at time = 200 s) as a function of the peptide/lipid molar ratio. ER-like vesicles (lipid concentration, 100 μM) were incubated with increasing doses of p7-C or p7-N (black and white circles, respectively). The V_0 value corresponds to the initial rate measured at a 1:50 peptide/lipid molar ratio. The peptide/lipid EC_{50} was inferred by fitting the experimental values of maximum leakage to a saturation curve. Depicted values are only applicable to the p7-C peptide. (B to E) Contribution of lipids in the ER-like mixture to pore-forming efficiency by p7-C peptide. (F and G) Effect of anionic phospholipids on p7-C pore-forming efficiency. In panels B to G experimental conditions were as in the right side of panel A. Mixtures of two lipids were equimolar.

virus replication and virulence. We demonstrated here that CSFV p7 possess an important pore formation activity, with maximal activity residing in the carboxyl half of the protein. We also show that the integrity of p7 is essential for the process of virus replication, and we mapped the specific areas of p7 critical for virus replication in cell cultures. In addition, we demonstrated that p7 plays a significant role in virulence during the infection in swine.

In accordance with results reported for BVDV (14), the integrity of p7 is decisive for CSFV production. Mutant CSFVs possessing three different partial in-frame deletions (two of them smaller

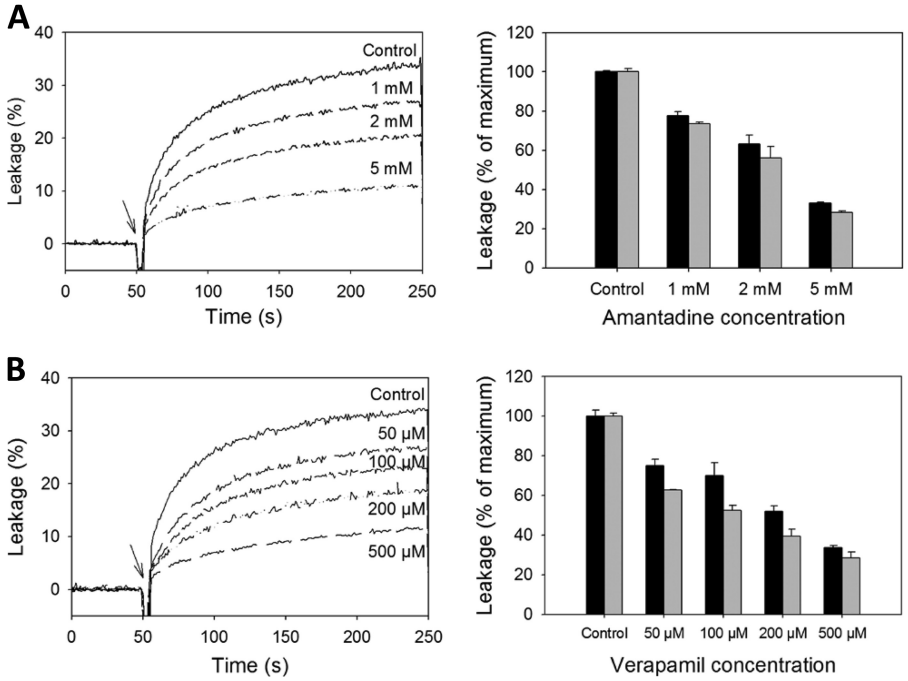

FIG 9 Effect of amantadine (A) and verapamil (B) on p7-C pore-forming activity. The left panels show the kinetic traces recorded after peptide addition to ER LUV (indicated by the arrow) in the presence of increasing amounts of the drugs. The peptide/lipid molar ratio was 1:50. The lipid concentration was 100 μM. The right panels show the percentage of maximum leakage and the initial rate (black and gray columns, respectively) as a function of the drug dose.

than that reported for BVDV) in the inner area of p7 were unable to grow in cell cultures. In contrast to what was observed with BVDV (14), CSFV mutant p7Δ15-51 failed to produce viral RNA after transfection, evidencing different roles for these residues between CSFV and BVDV. The importance of the integrity of p7 in the process of virus replication is demonstrated by the nonviability of CSFV constructs p7.2, p7.5, p7.9, p7.11, and p.7.12, where relatively small areas of the native sequence of the protein were substituted with alanine residues. Perhaps the role of CSFV p7 as a viroporin is critical in the process of virus replication, as has been shown for HCV p7 proteins (18, 29, 33). The significant sensitivity of CSFV to pore-forming inhibitors such as amantadine or verapamil supports this hypothesis.

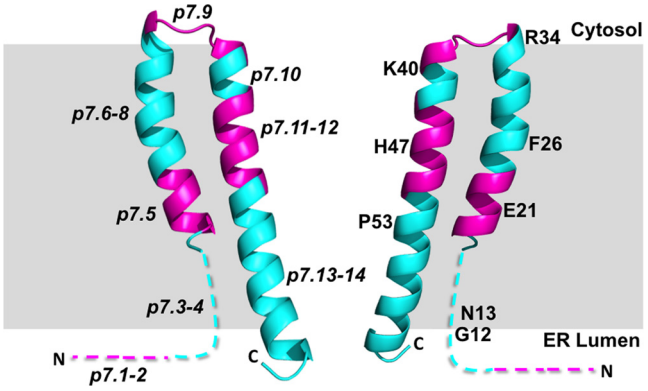

FIG 10 Predicted transmembrane topology of p7. The ER membrane is shown in gray, and the two predicted transmembrane helices are shown in ribbon diagrams with the N and C termini labeled. Two monomers are shown to indicate the predicted location of the pore; however, the model is not intended to show any oligomeric state. The extent of alanine constructs that resulted in nonviable viruses are shown in violet, and the remainder of the protein is shown in blue. The constructs are labeled p7.1–14 on the monomer on the left. The secondary, tertiary, and transmembrane helix prediction algorithms disagreed most strongly at the N-terminal 20 residues, so this region is represented as a dashed line. Residues discussed in the text are labeled on the p7 monomer shown on the left.

The role of CSFV p7 protein in the process of virus infection in the natural host has been largely ignored. This is the first report indicating a clear role for p7 in virulence in domestic swine. Mutations affecting areas p7.4, p7.8, p7.14, and, in particular, p7.10 significantly affect the ability of the viruses to produce disease. The mechanisms mediating this attenuation are not clear at this point. Perhaps it is the result of a decreased rate of replication, as demonstrated in primary swine macrophage cultures, which facilitates the host immune mechanisms that prevent the further dissemination of the virus. Although there is a correlation between the acquisition of attenuation in CSFV developed by reverse genetics and a certain degree of decreased ability to replicate in primary swine macrophage cultures (9, 26, 28), there are examples of attenuated viruses that replicate as efficiently as their virulent parental strain (10, 27). Further work will be necessary to assess other possible mechanisms producing virus attenuation.

Our experimental data (Fig. 5 to 9) and sequence-based secondary, tertiary, and topological predictions (Fig. 1 and 10) suggest that BICv p7 forms a channel, in which the C-terminal hydrophobic stretch is a pore lining transmembrane helix and the N-terminal hydrophobic stretch is of mixed secondary structure but containing a predominantly helical transmembrane segment with an unknown functional role in channel activity.

In the simplest model of the channel portion, in which a cytosolic loop centered on residues Arg34-Lys40 connects two transmembrane helices, four of the six conserved residues (Glu21, Phe26, His47, and Pro53) are predicted to be well within the membrane (Fig. 10). Two (His47 and Glu21) of these conserved, putative membrane-embedded residues are hydrophilic, and the alanine scanning data show that mutating the blocks containing either residue results in nonviable viruses, indicating that these residues may be involved in conductance. The latter, His47, may line the predicted pore in a similar fashion as His37 in the influenza virus M2 ion channel (16, 38). One of the few other residues in HCV p7 shown to be essential for p7 function, Tyr42 (33, 34), is in a transmembrane-embedded region similar in position to His47 of CSFV p7. Tyr42 and His47 are among the few strictly conserved amino acids in HCV p7s and pestivirus p7s, respectively. In HCV p7, alanine mutations of the dibasic motif, Lys33 and Arg35, prevent HCV replication in chimpanzees (29). The corresponding CSFV alanine construct, p7.9, did not produce infectious viruses. In both proteins, this region is predicted to form a cytosolic loop. Although sequence identity between the pestivirus p7 proteins and HCV p7 is low, our results suggest that these proteins are functionally similar and may in fact be similar to some extent at the structural level. Residue level comparisons between CSFV p7 and HCV p7 are informative, given the similar predicted structures and the wealth of data available for HCV p7; however, these comparisons must be interpreted with caution since the low homology of CSFV p7 to HCV p7 prevents direct extrapolation of functionality ascribed to HCV p7 amino acid residues to CSFV p7. Further experimental studies are needed to validate the CSFV p7 model presented here and to elucidate the role of invariant residues in pore formation and channel function.

In summary, we presented here novel experimental evidence for the role of CSFV p7 in the process of virus replication, pore formation, and virulence in swine. Further research is needed in order to examine in more detail the areas of the protein specifically responsible for each of these functions.

ACKNOWLEDGMENTS

We thank the Plum Island Animal Disease Center Animal Care Unit staff for excellent technical assistance. We also especially thank Melanie Prarat for editing the manuscript.

This research was partially supported by Spanish MCINN, Basque Government, and University of the Basque Country grants (BIO2011-29792 and GIU 06/42 to J.L.N.).

REFERENCES

1. **Acharya R, et al.** 2010. Structure and mechanism of proton transport through the transmembrane tetrameric M2 protein bundle of the influenza A virus. Proc. Natl. Acad. Sci. U. S. A. **107**:15075–15080.
2. **Barth P, Schonbrun J, Baker D.** 2007. Toward high-resolution prediction and design of transmembrane helical protein structures. Proc. Natl. Acad. Sci. U. S. A. **104**:15682–15687.
3. **Becher P, et al.** 2003. Genetic and antigenic characterization of novel pestivirus genotypes: implications for classification. Virology **311**:96–104.
4. **Borca MV, Gudmundsdottir I, Fernandez-Sainz IJ, Holinka LG, Risatti GR.** 2008. Patterns of cellular gene expression in swine macrophages infected with highly virulent classical swine fever virus strain Brescia. Virus Res. **138**:89–96.
5. **Carrere-Kremer S, et al.** 2002. Subcellular localization and topology of the p7 polypeptide of hepatitis C virus. J. Virol. **76**:3720–3730.
6. **Edwards S, Moennig V, Wensvoort G.** 1991. The development of an international reference panel of monoclonal antibodies for the differentiation of hog cholera virus from other pestiviruses. Vet. Microbiol. **29**:101–108.
7. **Elbers K, et al.** 1996. Processing in the pestivirus E2-NS2 region: identification of proteins p7 and E2p7. J. Virol. **70**:4131–4135.
8. **Ellens H, Bentz J, Szoka FC.** 1985. H^+- and Ca^{2+}-induced fusion and destabilization of liposomes. Biochemistry **24**:3099–3106.
9. **Fernandez-Sainz I, et al.** 2010. Mutations in classical swine fever virus NS4B affect virulence in swine. J. Virol. **84**:1536–1549.
10. **Gallei A, et al.** 2008. Cytopathogenicity of classical swine fever virus correlates with attenuation in the natural host. J. Virol. **82**:9717–9729.
11. **Gonzalez ME, Carrasco L.** 2003. Viroporins. FEBS Lett. **552**:28–34.
12. **Griffin SD, et al.** 2003. The p7 protein of hepatitis C virus forms an ion channel that is blocked by the antiviral drug, amantadine. FEBS Lett. **535**:34–38.
13. **Griffin SD, et al.** 2004. A conserved basic loop in hepatitis C virus p7 protein is required for amantadine-sensitive ion channel activity in mammalian cells but is dispensable for localization to mitochondria. J. Gen. Virol. **85**:451–461.
14. **Harada T, Tautz N, Thiel HJ.** 2000. E2-p7 region of the bovine viral diarrhea virus polyprotein: processing and functional studies. J. Virol. **74**:9498–9506.
15. **Hope MJ, et al.** 1985. Production of large unilamellar vesicles by a rapid extrusion procedure: characterization of size distribution, trapped volume, and ability to maintain a membrane potential. Biochim. Biophys. Acta **812**:55–65.
16. **Hu F, Luo W, Hong M.** 2010. Mechanisms of proton conduction and gating in influenza M2 proton channels from solid-state NMR. Science **330**:505–508.
17. **Huarte N, et al.** 2008. The broadly neutralizing anti-human immunodeficiency virus type 1 4E10 monoclonal antibody is better adapted to membrane-bound epitope recognition and blocking than 2F5. J. Virol. **82**:8986–8996.
18. **Jones CT, Murray CL, Eastman DK, Tassello J, Rice CM.** 2007. Hepatitis C virus p7 and NS2 proteins are essential for production of infectious virus. J. Virol. **81**:8374–8383.
19. **Karplus K.** 2009. SAM-T08, HMM-based protein structure prediction. Nucleic Acids Res. **37**:W492–W497.
20. **Lamp B, et al.** Biosynthesis of classical swine fever virus nonstructural proteins. J. Virol. **85**:3607–3620.
21. **Luscombe CA, et al.** 2010. A novel hepatitis C virus p7 ion channel inhibitor, BIT225, inhibits bovine viral diarrhea virus in vitro and shows synergism with recombinant interferon-α-2b and nucleoside analogues. Antivir. Res. **86**:144–153.
22. **McGuffin LJ, Bryson K, Jones DT.** 2000. The PSIPRED protein structure prediction server. Bioinformatics **16**:404–405.
23. **Mittelholzer C, Moser C, Tratschin JD, Hofmann MA.** 2000. Analysis of classical swine fever virus replication kinetics allows differentiation of highly virulent from avirulent strains. Vet. Microbiol. **74**:293–308.
24. **Phillips R, Ursell T, Wiggins P, Sens P.** 2009. Emerging roles for lipids in shaping membrane-protein function. Nature **459**:379–385.
25. **Reed LJ, Muench HA.** 1938. A simple method of estimating fifty per cent endpoints. Am. J. Hyg. **27**:493–497.
26. **Risatti GR, et al.** 2005. The E2 glycoprotein of classical swine fever virus is a virulence determinant in swine. J. Virol. **79**:3787–3796.
27. **Risatti GR, et al.** 2005. Mutation of E1 glycoprotein of classical swine fever virus affects viral virulence in swine. Virology **343**:116–127.
28. **Sainz IF, Holinka LG, Lu Z, Risatti GR, Borca MV.** 2008. Removal of a N-linked glycosylation site of classical swine fever virus strain Brescia Erns glycoprotein affects virulence in swine. Virology **370**:122–129.
29. **Sakai A, et al.** 2003. The p7 polypeptide of hepatitis C virus is critical for infectivity and contains functionally important genotype-specific sequences. Proc. Natl. Acad. Sci. U. S. A. **100**:11646–11651.
30. **Sanger F, Nicklen S, Coulson AR.** 1977. DNA sequencing with chain-terminating inhibitors. Proc. Natl. Acad. Sci. U. S. A. **74**:5463–5467.
31. **Sonnhammer EL, von Heijne G, Krogh A.** 1998. A hidden Markov model for predicting transmembrane helices in protein sequences. Proc. Int. Conf. Intell. Syst. Mol. Biol. **6**:175–182.
32. **Sreerama N, Woody RW.** 2000. Estimation of protein secondary structure from circular dichroism spectra: comparison of CONTIN, SELCON, and CDSSTR methods with an expanded reference set. Anal. Biochem. **287**:252–260.

33. **Steinmann E, et al.** 2007. Hepatitis C virus p7 protein is crucial for assembly and release of infectious virions. PLoS Pathog. **3**:e103.
34. **St Gelais C, et al.** 2009. Determinants of hepatitis C virus p7 ion channel function and drug sensitivity identified in vitro. J. Virol. **83**: 7970–7981.
35. **Terpstra C, Woortmeyer R, Barteling SJ.** 1990. Development and properties of a cell culture produced vaccine for hog cholera based on the Chinese strain. Dtsch. Tierarztl. Wochenschr. **97**:77–79.
36. **Thiel HJ, Stark R, Weiland E, Rumenapf T, Meyers G.** 1991. Hog cholera virus: molecular composition of virions from a pestivirus. J. Virol. **65**:4705–4712.
37. **van Meer G, Voelker DR, Feigenson GW.** 2008. Membrane lipids: where they are and how they behave. Nat. Rev. Mol. Cell. Biol. **9**:112–124.
38. **Venkataraman P, Lamb RA, Pinto LH.** 2005. Chemical rescue of histidine selectivity filter mutants of the M2 ion channel of influenza A virus. J. Biol. Chem. **280**:21463–21472.
39. **Viklund H, Bernsel A, Skwark M, Elofsson A.** 2008. SPOCTOPUS: a combined predictor of signal peptides and membrane protein topology. Bioinformatics **24**:2928–2929.
40. **Zsak L, Lu Z, Kutish GF, Neilan JG, Rock DL.** 1996. An African swine fever virus virulence-associated gene NL-S with similarity to the herpes simplex virus ICP34.5 gene. J. Virol. **70**:8865–8871.